Results in Engineering 17 (2023) 100852

Contents lists available at ScienceDirect

Results in Engineering

journal homepage: www.sciencedirect.com/journal/results-in-engineering

Full Length Article

Mining of deep-seabed nodules using a Coandă-effect-based collector

Said Alhaddad [a,*], Dhruv Mehta [b], Rudy Helmons [a,c]

[a] Section of Offshore and Dredging Engineering, Faculty of Mechanical, Maritime and Materials Engineering, Delft University of Technology, Delft, the Netherlands
[b] Department of Water Management, Faculty of Civil Engineering and Geoscience, Delft University of Technology, Delft, the Netherlands
[c] Department of Mineral Processing and HSE, Norwegian University of Science and Technology, Trondheim, Norway

ARTICLE INFO

Keywords:
Deep sea mining
Polymetallic nodules
Hydraulic collector
Coandă effect
Nodule pick-up device

ABSTRACT

We present an effective design of a hydraulic, polymetallic nodule collector, which fundamentally depends on the Coandă effect in harvesting nodules. The design was first developed based on 2D numerical simulations conducted using a computational fluid dynamics tool, ANSYS FLUENT. Following that, the design was tested in full-scale experiments, which provided insights into the collection efficiency of the collector and confirmed its functionality and effectiveness. The latter means, in the context of deep sea mining, high effective pick-up of nodules, with minimum sediment disturbance. Our observations indicate that our design hardly disturbs the tested sediment bed. The experimental results show that a higher jet velocity leads to a higher pick-up efficiency. Two forward velocities were tested and the higher forward velocity led to a lower pick-up efficiency. It is revealed that the available time for the nodules to respond to the pressure gradient under the collector is of great importance; if the available time is not sufficient, the nodules will not be picked-up even if the pressure gradient is adequate. The clearance under the rear cowl of the collection duct is found to play a major influential role in the collection process; a smaller bottom clearance results in a higher pick-up efficiency.

1. Introduction

The demand for critical materials, such as cobalt and lithium is constantly growing worldwide. This is highly driven by growing populations, urbanization and ongoing development of technology [12], in particular the green transition, which is mainly driven by an increase in renewable energy capacity and the electrification of the automotive industry. Recently, IEA [15] analyzed various scenarios, i.e. Current Stated Policies (STEPS) and Net Zero Emissions (NZE) by 2050. According to these scenarios, the expected growth in demand by 2040 for Cu, Ni and Co is for STEPS 31%, 73% and 143%, respectively, and for NZE 40%, 168% and 372%, respectively.

Nowadays, there is an increased global attention to the potential of deep sea as an unexploited resource of several key raw materials and an alternative to terrestrial deposits. Immense quantities of strategic metals are present on the seabed, for instance, 83% of the total global cobalt rests untouched on the bottom of the ocean (54% in polymetallic nodules) [21]. Polymetallic nodules are potato-shaped concretions, which occur on the seabed in most oceans around the world and contain large quantities of critical metals (e.g. copper, nickel and cobalt) and rare earth elements. Enormous tonnage of these nodules, in particular, are available on the seabed within the Clarion Clipperton Zone (CCZ) in the Pacific Ocean and the Indian Ocean Nodule Field [12] at typical water depths of 4-6 km. These nodules are often partly or completely buried in the seabed sediment, which is mainly composed of clay or ooze-like sediment (see Fig. 1). Field experiments conducted by Global Sea Mineral Resources NV in the eastern part of the CCZ demonstrated that the average grain diameter of the sediment d_{50} is 0.012 mm and the bulk density ranges from 1250 kg/m^3 to 1450 kg/m^3 [10].

Currently, there are several studies underway to evaluate the economic and technical feasibility for exploitation of polymetallic nodules, as well as assessing the ecological risks involved [11,6,20,7,10,18]. The main tasks of a polymetallic nodule collector are (i) collecting the nodules present on the seabed (ii) separating nodules from sediments and (iii) supplying nodules to the riser system to transport them to the sea surface. There are three main mechanisms for mining polymetallic nodules: mechanical, hydraulic and hybrid (Fig. 2). Mechanical collectors involve moving parts to pick-up and convey the nodules; they use rotating scoops and dig into the upper part of the seabed to harvest the nodules and then they transport the nodules to a conveyor belt. In contrast, hydraulic collectors do not directly get in contact with the nodules nor with the sediments. However, they produce a pressure difference to pick-up the nodules, thus considerably minimising the disturbance to the seabed environment. Hybrid-type collectors combine the mechan-

* Corresponding author.
E-mail addresses: S.M.S.Alhaddad@tudelft.nl (S. Alhaddad), D.Mehta@tudelft.nl (D. Mehta), R.L.J.Helmons@tudelft.nl (R. Helmons).

https://doi.org/10.1016/j.rineng.2022.100852
Received 19 October 2022; Received in revised form 14 December 2022; Accepted 16 December 2022
Available online 21 December 2022

Fig. 1. Undisturbed nodule-sediment sample illustrating the burial of nodules (Museum National d'Histoire Naturelle Box Corer [19]).

ical and hydraulic mechanisms, where the nodules are hydraulically dislodged from the bed and then transported by a mechanical conveyor [14,13].

Environmental impact of deep sea mining is one of the current major concerns [3,8]. From an environmental viewpoint, hydraulic collecting is the most preferred technology in deep sea mining. This is because it barely involves interaction with the seabed during nodules harvesting [1]. Besides, the results of a sea test conducted in 1978 showed that the hydraulic method results in a higher pick-up efficiency than the mechanical method [17]. Additionally, hydraulic systems consume less power than mechanical systems [4]. Furthermore, hydraulic methods show a better adaptability to the variations in the seabed bathymetry than the other methods [26], motivating further development of this mechanism. The working principle of the collector is to create a flow of water over nodules on the seabed, which exerts both lift and drag forces on the nodules. The lift force moves the nodules in the vertical direction, while the drag force pushes the nodules into the collection duct of the collector. Following that, in some designs, a stream of clean water is used to separate the nodules from the suspended sediment, minimizing the amount of sediments entering the vertical transport system. Keeping sediments down at the seabed is environmentally desirable, since it keeps the suspended sediment plume more confined to the vicinity of the mining area. Besides, it is desirable from a cost efficiency perspective, as it limits unnecessary transport of unwanted material.

Nodule collector devices are primarily evaluated based on their nodule pick-up efficiency, which depends on several factors, such as nodule size, jet velocity, forward velocity of the collector and bottom clearance. In this paper, we present an effective design of a hydraulic collector, which was first developed based on 2D numerical simulations run using a computational fluid dynamics (CFD) tool, ANSYS FLUENT. As a follow-up, a set of full-scale experiments has been conducted to obtain a deeper insight into the collection efficiency of the hydraulic collector under different operational conditions and to develop a better understanding of the underlying physics of the collection process. The results of the numerical simulations and lab experiments are presented and discussed.

2. Design principle

A hydraulic collector is a system that uses water/sediment-water mixture to collect nodules and transport them to a separator, where nodules settle down. Compared with other hydraulic collection methods, the Coandă-effect-based method is the most promising method in terms of pick-up efficiency and flow field disturbance [24]. Therefore, the design we present here fundamentally depends on the Coandă effect in collecting nodules. Coandă effect is a fascinating phenomenon in the field of fluid mechanics, which was discovered by the Romanian scientist Henri Coandă. This effect can be described as the property of a jet flow to adhere to an adjacent surface and also to keep adhering when the surface curves. Fig. 3 shows a schematic of the basic design of a Coandă-effect-based collector. It comprises three concentric surfaces that form two ducts: jet duct and a collection duct. The former is for a high velocity jet of water that follows the curvature of the upper plate as a result of the Coandă effect. This brings about an entrainment of the surrounding water towards the upper plate, which creates a suction that could dislodge a nodule from the seabed and carry it towards the collection duct.

Recent works have analyzed design of such collector systems, [e.g., 16,5]. A prototype Coandă-effect-based collector has been developed and tested by Cho et al. [5], with the emphasis to link the collector performance to a tracked vehicle on analyzing the integrated design. Although lab tests are presented, no significant data is presented regarding its pick-up performance. Jia et al. [16] have analyzed three types of hydraulic collector systems, i.e., suck-up based, Coandă-effect based and double row hydraulic sluicing. The performance of the three systems is compared numerically and, unfortunately, no experimental validation is presented. Zhao et al. [25] studied another hydraulic collector principle, based on a spiral flow to pick up individual nodules. This study was based on numerical simulations and validated through lab-scale experiments to analyze the suction flow field. Weaver et al. [22] provided an overview of collector systems in various stages of product development, ranging from concept to pilot testing in the Clarion Clipperton Zone. The technical performance of these systems is either not yet tested, or has not (yet) been made publicly available.

Our objective in this study is to develop a collector head with an optimal pick-up efficiency while maintaining a minimal environmental impact. To this end, a deep understanding of the phenomena occurring during nodules pick-up is required. Our strategy is to minimise the water flow for two reasons. Firstly, flow rate is directly related to the power required for the pumps and the corresponding costs are proportional. Secondly, water flow near the seabed generates a sediment plume, which, from an environmental point of view, should be minimized as much as possible. This study is unique, as we provide design considerations based on CFD and we tested our collector in a full-scale laboratory setup.

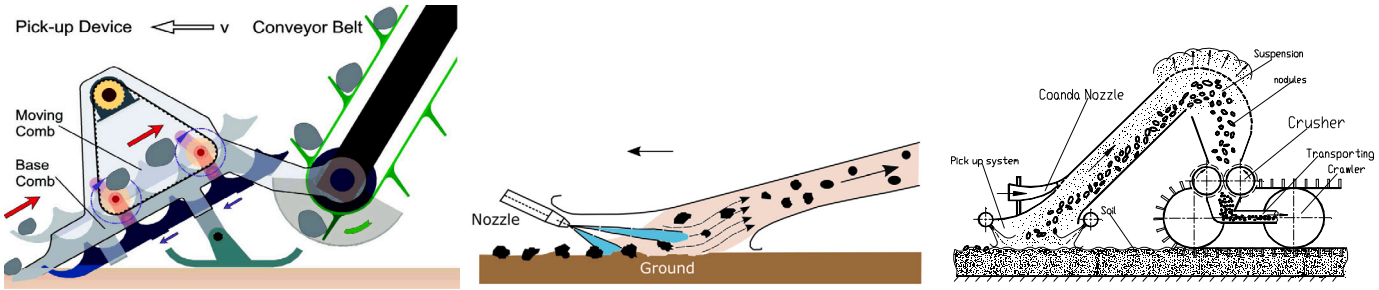

Fig. 2. Mechanisms to collect polymetallic nodules: mechanical (**left**), hydraulic (**middle**) [4] and hybrid (**right**) [23].

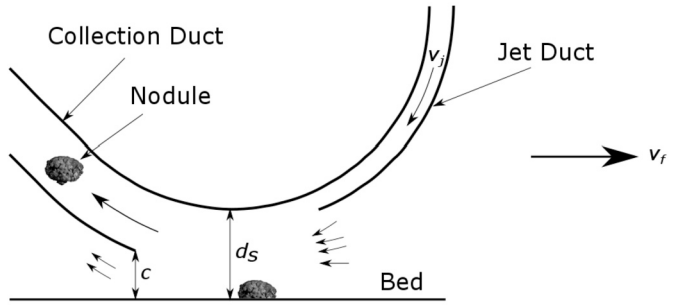

Fig. 3. Schematic representation of the collector head; v_j is the jet velocity, v_f is the forward velocity of the collector and c is clearance. The smallest arrows depict the direction of water entrainment.

3. Computational fluid dynamics (CFD)-based design

The generic design in Fig. 3 must be optimised for the effective collection of nodules, within the limits of available power and permissible impact on the ocean floor. A completely experimental optimisation is expensive, given the numerous parameters influencing the collector's efficiency, ranging from dimensions and jet velocity to the clearance from the seafloor. Thus, CFD was used as a numerical alternative to create an optimised design that could later be prototyped for experimentation.

ANSYS FLUENT was chosen as the solver for its robustness and ease of operation, which included quick visualisation of the results and post-processing. All computational meshes were created with ANSYS ICEM CFD using two dimensional (2-D) sections of the hydraulic collector, as shown in Fig. 3. The $\kappa - \epsilon$ model was chosen for turbulence (single phase flow), the pressure-implicit with splitting of operator (PISO) scheme was used for pressure-velocity coupling and the discretisation was second order accurate in space and the solution was advanced in time with a second order implicit scheme. The Reynolds numbers in our case, are calculated with respect to the jet, which is the major source of momentum in the region of interest (underside of the collector). The range we have analysed is between 100,000 to 200,000 based on the jet velocity, the slot width of the jet and the density and viscosity of seawater.

It is worth noting that the CFD process is mainly to achieve an optimised design that could be fabricated and tested in a laboratory and later in the field. Therefore, the CFD itself will not be validated but the design so-suggested will be thoroughly evaluated and improved through laboratory improvements. In this case, CFD helps to provide the first guess of what an efficient design could be.

3.1. Methods

Fig. 4 shows how the collector is meshed inside a domain that is open on the left, right and at the top, with the bottom acting as the seafloor. A close-up of the main operational region is shown in Fig. 5, wherein the jet duct is the narrow one on the right and the collection duct is the wide one on the left. The collector moves over the seafloor from left to right.

The collector is simulated inside a domain (2-D) that is nearly 13 m long and 6 m high, with the collector being 2.5 m long (along the x-axis between the furthest points at the back and the front). The same dimension along the y-axis is 1.5 m. All boundaries are stress-free boundaries (except the seafloor that is a wall), which permit the water from the duct to blend smoothly with the surrounding water and leaving the domain through the stress-free boundaries. The seawater has a density of 1028 $\mathrm{kg\,m^{-3}}$ and a viscosity of 0.00167 Pa s pertinent to a depth of 6 km.

The mesh is unstructured for easy adaptation to the curved surfaces of the collector and comprises triangular elements filling up the surface

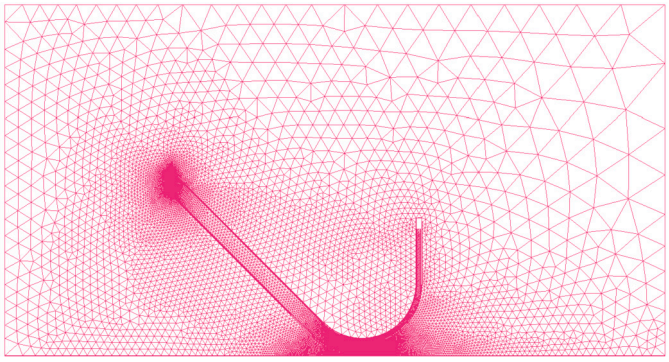

Fig. 4. A 2-D unstructured mesh of the collector.

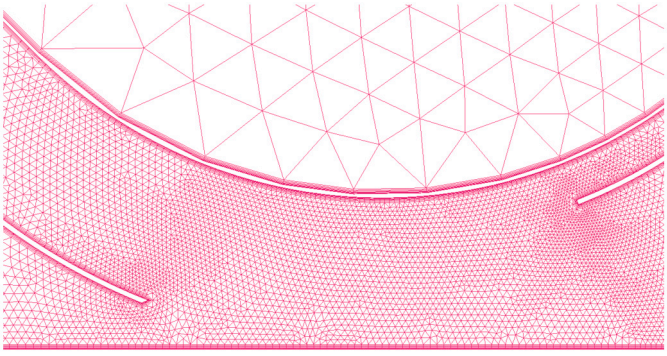

Fig. 5. Boundary layer elements for the mesh shown in Fig. 4.

that represents the seawater. Further, quadrilateral mesh elements are used to simulate the boundary layer that would develop over collector's surfaces and the seafloor. As experimental data was unavailable, grid convergence was assessed as grid independence. The contours of velocity such as those in Fig. 8 were used as a reference. The grid was successively refined (factor of 2) until the contours (when interpolated from a finer grid onto a coarser one) had an average relative change of less than 0.05. This number was chosen to represent the so-called 'asymptotic range' due to limits on computational power that precluded the simulation of highly-refined meshes.

To account for the collector's forward motion, the collector has been modelled as stationary while the flow enters the domain from the right side with a velocity equal to the collector's forward velocity. The surfaces on the top and back have a stress-free boundary condition with only the pressure explicitly specified as the hydrostatic pressure. The white block in the middle of the domain is used to isolate the jet's inlet boundary with a velocity condition imposed on it. The two velocity inlets, the front of the domain and the jet, were modelled as being fully turbulent. The Reynolds number in the case of the front inlet was calculated with the collector's forward velocity and vertical dimension (in 2-D), while that for the jet was obtained using the jet velocity and diameter.

Although the simulations are carried out in 2-D for simplicity, the collector in reality is a 3-D structure. During a mining campaign, multiple individual collectors, next to each other, will be used simultaneously, where every collector (or 'unit') is 1 m wide. Depending on the number of these units, the overall collective width is expected to be around 10-20 m in width. This means that the seawater above the collector, below it and on its sides, forms a continuous volume. So, any distortion to this volume is borne by the continuity of the seawater around the jet, in a 3-D manner. Hence, the collection duct was kept open at its rear-end, forcing it to empty its content into the seawater, to ensure that the continuity of the volume of seawater around the collector in 3-D is maintained in its 2-D equivalent. The collection duct

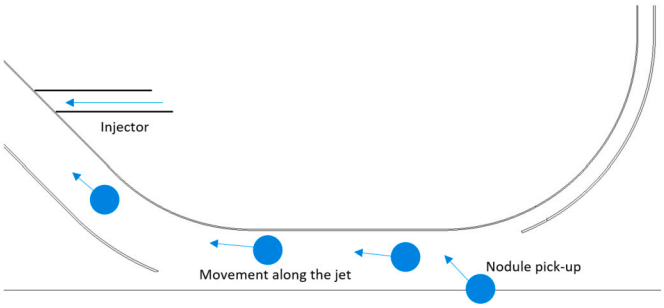

Fig. 6. A collector with a flat underside.

has been elongated to offer sufficient resistance to the incoming flow (assessed *a posteriori*) and mimic the downstream components of the collector (separator, diffuser and the conduits in between). The domain itself is much larger as compared to the collector. This is to ensure that the water leaving the open duct at the bottom is not restricted in any manner, affecting the flow inside the duct.

Validation is done using laboratory tests wherein, the prototype is able to abstract nodules and maintain a constant flow through the collection duct and the diffuser at the rear, demonstrating that the latter does not provide a very high back pressure to disrupt the flow under the collector. The CFD process was then updated with a suitable design for the collector, separator and diffuser as one unit, following which, a final prototype was created for the experiments that will be described later in this article.

3.2. Summary of the optimisation routine

To begin with, the power available for the jet was limited, in turn limiting the jet's velocity to a maximum of 10 ms^{-1} (simulations with higher velocities were performed to assess robustness). The widths of the jet and collection ducts were chosen to maintain sufficient clearance from the seafloor and nodules.

This section provides a measure of the impacts of the jet velocity, collector's forward velocity, the shape of the collector's underside along which the jet flows and the presence of an injector in the collection duct. The duct height is 20 mm and the jet flows is primarily tested for velocities between 5 and 10 ms^{-1}.

3.2.1. Underside design

The movement of the jet along the underside shown in Fig. 3 leads to the entrainment of seawater as a consequence of the Coandă effect. This creates a region of low pressure that extracts the nodules from the seafloor. However, the nodules need some time to get extracted and move into the collection duct. If this time is not available, the nodules may not traverse the vertical distance needed to clear the cowl at the bottom of the collection duct. Therefore, an alternative design with a slightly extended underside, as shown in Fig. 6, was also considered.

The contours of velocity and static pressure are shown in Fig. 7 and Fig. 8. The Coandă effect is diffused over the flat region, which, due to the transit time itself, leads to an increase in the amount of seawater that the jet entrains and hence, an overall faster velocity field under the collector. On the other hand, the contours of static pressure reveal that the pressure gradient is stronger for a curved underside.

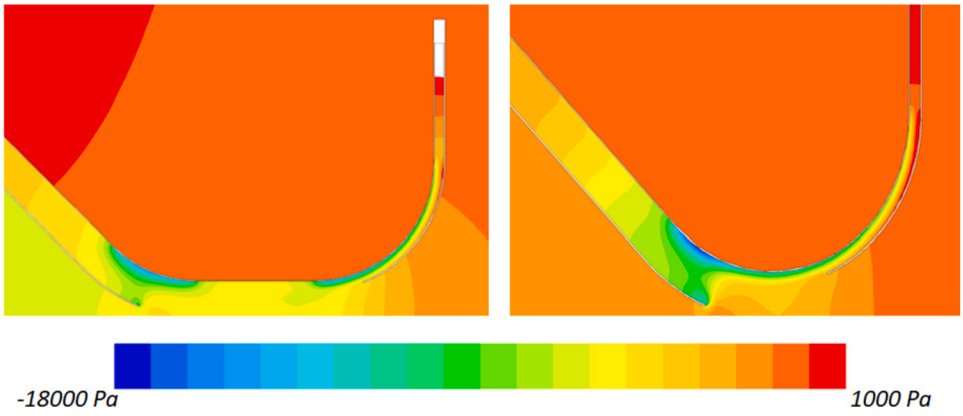

Fig. 7. Pressure contours for a flat (**left**) and curved underside (**right**) for the maximum jet velocity of 10 ms^{-1}.

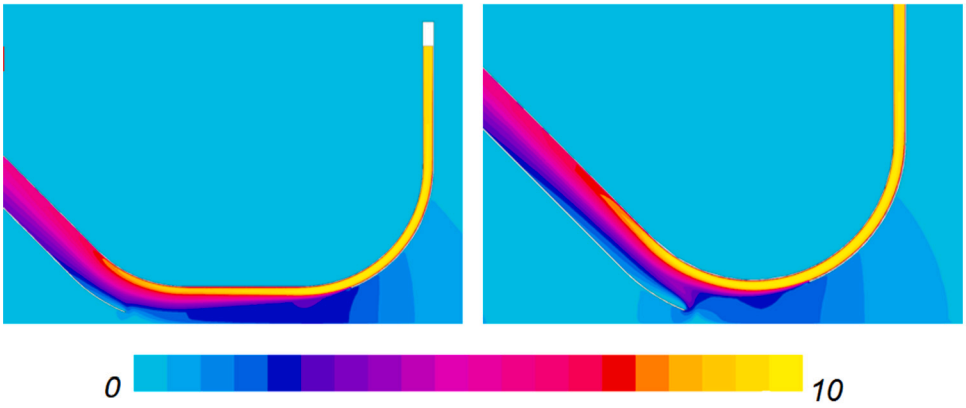

Fig. 8. Velocity contours for a flat (**left**) and curved underside (**right**).

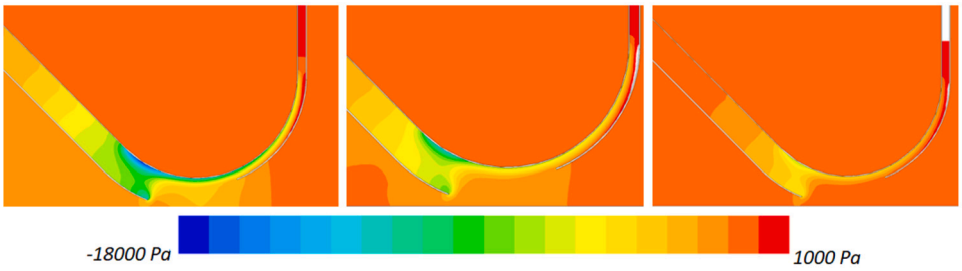

Fig. 9. Pressure contours for various velocities of the main jet. From left to right, 10, 8 and 6 ms^{-1}.

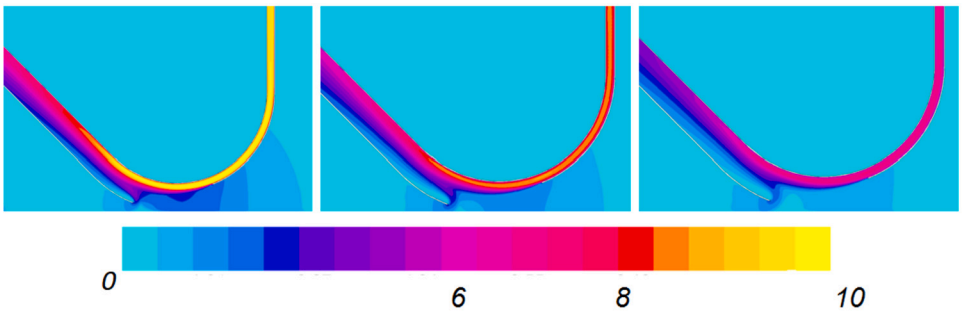

Fig. 10. Velocity contours for various velocities of the main jet. From left to right, 10, 8 and 6 ms^{-1}.

The net force on an imaginary nodule was calculated as the difference between the suction generated by the collector on the surface of the nodule (pressure contours) and the adhesion of the nodules to the sediment. A positive value would indicate that a nodule could be dislodged from the seafloor. Using this as a reference, it was concluded that for the power available in our case, only a curved underside could generate sufficient suction to dislodge a nodule.

3.2.2. Jet velocity

Contours of velocity and static pressure for different jet velocities are shown in Fig. 9 and Fig. 10, respectively. Reducing the jet velocity leads to reduced entrainment and a slower velocity field. As a result, the pressure gradient under the collector is also weakened. By assessing the difference between the pressure on the seafloor (due to the collector) and the adhesive force between the nodules and the seafloor, it was concluded that even 8 ms^{-1} is not sufficient to dislodge nodules. A velocity higher than 10 ms^{-1} brings about a larger pressure difference but requires more energy.

3.2.3. Collector's forward velocity

The collector's forward velocity is a critical component of the design for two reasons. Firstly, it leads to compression of the water in front of the collector (similar to a jet engine that moves through air), building up a high pressure that eventually leads to a larger gradient underneath the collector at a given jet velocity. Secondly, the forward velocity influences the duration over which the collector's underside remains over a nodule and attempts to pull it out of the seabed through the suction created by the jet; a faster forward moving collector will influence a nodule for a shorter duration as it passes over the same. Hence, a high forward velocity will create a stronger suction, but the collector can pass rather quickly over a nodule, providing little time for extraction and traversing the vertical distance needed to clear the rear cowl (see Fig. 3). Further, maintaining a higher forward velocity requires overcoming more drag from the surrounding water and hence may not be feasible given the limited amount of power available. Increasing the velocity directly increases the pressure gradient (and suction) on the underside. This combined with the fact that a higher forward velocity is economically more favourable for covering larger areas of the seafloor in a given time, led to the choice of 0.5 ms^{-1} as the baseline operating velocity.

3.2.4. Injectors

Once picked up, it is essential to ensure that the nodules move up the collection duct into a downstream separation unit, while overcoming any resistance that might arise. Therefore, the effect of injecting additional water (from the surroundings) into the collection duct, slightly downstream of its mouth, was also explored as part of the design process. An injector provides additional propulsion to move the nodules (heavy ones) up the duct. Two widths were considered, $D_{i1} = 40$ mm and $D_{i2} = 5$ mm. D_{i1} is equal to the width of the jet, whereas D_{i2} is one-eighth of D_{i1}. The flow velocities through D_{i1} were lower than 10 ms^{-1} at 2, 4 and 6 ms^{-1}. Whereas, the velocities through D_{i2} where higher than 10 ms^{-1} at 20, 30 and 40 ms^{-1}. The mass flow rates were eventually comparable however, D_{i2} provided a larger amount of momentum and energy. Apart from providing propulsion to the nodules, these injectors acted as secondary ducts that could bring about the Coandă effect and entrain more water from the region under the collector, leading to a larger suction and by extension, a better pickup performance.

However, D_{i1} was unable to create this effect. The addition of a large volume of water in fact, increased the pressure in the duct leading to a negative influence on the suction, solely due to the excess mass in the duct. Fig. 11 and Fig. 12 show this effect through contours of velocity and pressure. In contrast, injecting the same volume of water at very high velocities, led to increased entrainment and a marked reduction in pressure on the underside of the collector. Despite this advantage, these thin injectors were not considered due to the power requirements that exceed those of the main jet itself.

4. Full-scale experiments

Based on the schematic shown in Fig. 3 and the insights obtained from the numerical simulations presented in the previous section, full-scale experiments were conducted. This section describes the experimental setup, instrumentation, experimental procedure and data processing, and lastly discusses the experimental results.

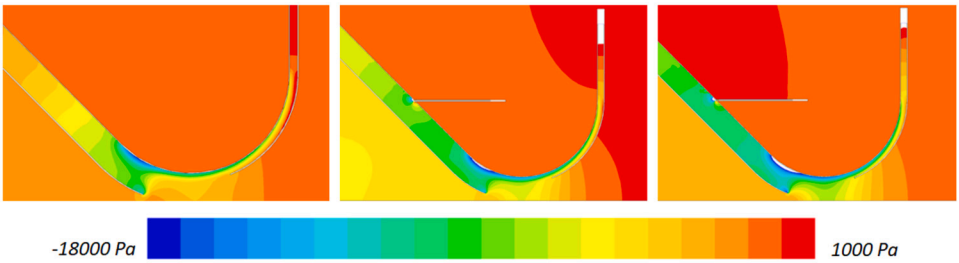

Fig. 11. Pressure contours for various injection velocities. From left to right, 0, 20 and 30 ms^{-1}.

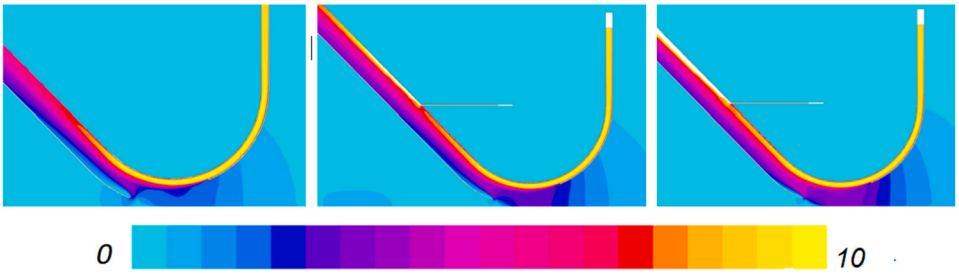

Fig. 12. Velocity contours for various injection velocities. From left to right, 0, 20 and 30 ms^{-1}.

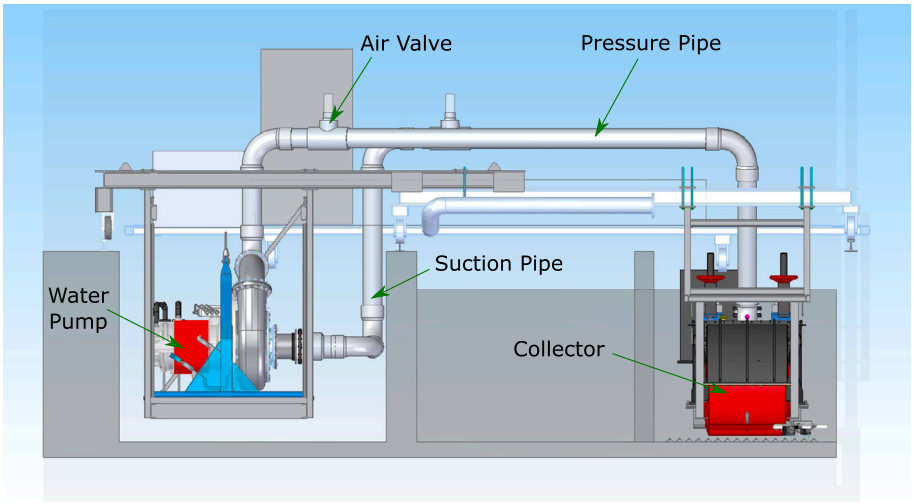

Fig. 13. 2D computer model of the experimental setup.

4.1. Experimental setup

The experimental setup consists of several components: the collector, pipes, a water pump, two water flumes and a testing track. A description of each component of the experimental setup is provided in the subsequent paragraphs.

4.1.1. The collector

The collector consists mainly of a jet duct (height = 20 mm), a collection duct (height = 150 mm) and a discharge pipe. The collector was fastened on a mobile carriage, which operates on rails and can move at the required forward velocity.

4.1.2. Pipes and water pump

The collector was connected to a water pump through two PVC pipes (Fig. 13): a suction pipe and a pressure pipe (diameter = 250 mm). The former is used to get the water from the ambient water and the latter is used to feed the jet with water or sediment-water mixture. A variable frequency drive was used to control the frequency of the electrical power supplied to the pump.

4.1.3. Water flumes and testing track

The experimental setup involves two water flumes: a flume where the tests with the collector are conducted (termed hereafter as the 'testing flume') and another flume where the water pump is installed (termed hereafter as the 'pump flume'). The latter was needed, because the pump used operates only underwater. The testing flume is 31.25 m long, 2.40 m wide and 2.50 m high, while the pump flume is 33 m long, 3.5 m wide and 2.5 m high. Fig. 14 shows the top view of the experimental setup when the water flumes are filled with water.

The testing track (19.5 m long and 1.22 m wide) was constructed in the middle of the testing flume using planks to accommodate the sand bed (see Fig. 15). The rationale behind this track is to reduce the amount of sand required for a test, to facilitate the process of leveling the sand bed and to correctly mount the nodules in the path of the collector.

In reality, polymetallic nodules are often partly buried in the seabed sediment, which is mainly composed of clay. Nevertheless, the current experiments were conducted using sand instead, so as to allow the execution of a larger number of tests and to investigate more scenarios.

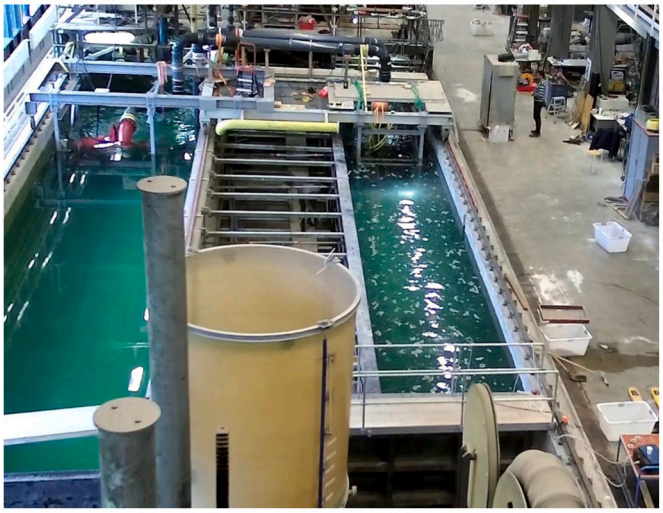

Fig. 14. Top view of the experimental setup showing the pump flume (left one) and the testing flume (right one).

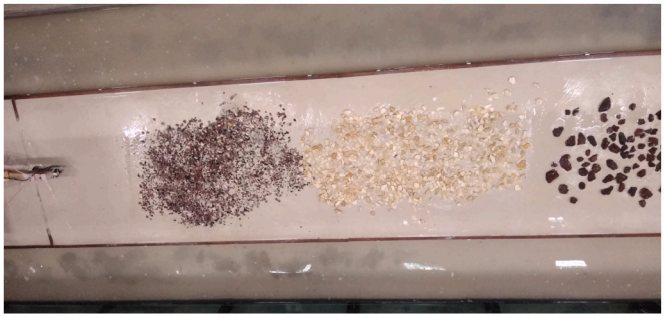

Fig. 15. The testing track filled with 15 cm sand into which nodules are half buried.

4.2. Test procedure

To understand the effect of the critical parameters on the pick-up process, the experiments were conducted according to a predefined sequence in which the complexity gradually increases as follows:

(i) stationary collector without nodules,
(ii) moving collector over a rigid bed without nodules,
(iii) moving collector over a rigid bed with nodules,
(iv) moving collector over a sand bed without nodules,
(v) moving collector over a sand bed with nodules.

The experiments were prepared following the next sequence of steps:

- The elevation of the hydraulic collector is adjusted to the targeted clearance. To allow for two clearances in the same run, in the case of a rigid bed, wooden plates (2.5 cm thick) are placed on the flume bed in the first half of the collector path (see Fig. 16 left).
- In the case of a sand bed, sand is mounted inside the testing track until reaching a depth of 15 cm. Following that, the sand bed is leveled using a wooden plank.
- Batches of nodules are prepared and placed on the flume bed with an abundance (the mass of nodules per unit area) of 15 kg/m^2. In the case of a sand bed, the nodules are pushed inside the sand until almost half of their area is still extruding.
- The water flumes are filled with water.
- The air valves are opened and the vacuum pump is turned on to remove the air from the system. The air valves are closed once the air is pumped out.
- Simultaneously with the previous step, the water pump is switched on at the frequency needed to operate at the targeted jet velocity.

After testing the signal of the measurement instruments, the experiment proceeds as follows:

- The mobile carriage drives at the specified forward velocity (25 cm/s or 50 cm/s) and eventually stops and the end of the testing track.
- The flume water is totally drained.
- The nodules remaining on the flume bed are manually collected, washed and weighed to calculate the pick-up efficiency, which is defined as the ratio of the mass of collected nodules to the mass of nodules available for collection.

4.3. Instrumentation

The experimental setup was equipped with many sensors to collect local measurements of flow rate, flow pressure, flow velocity and particle concentration. To measure the flow rate, two electromagnetic

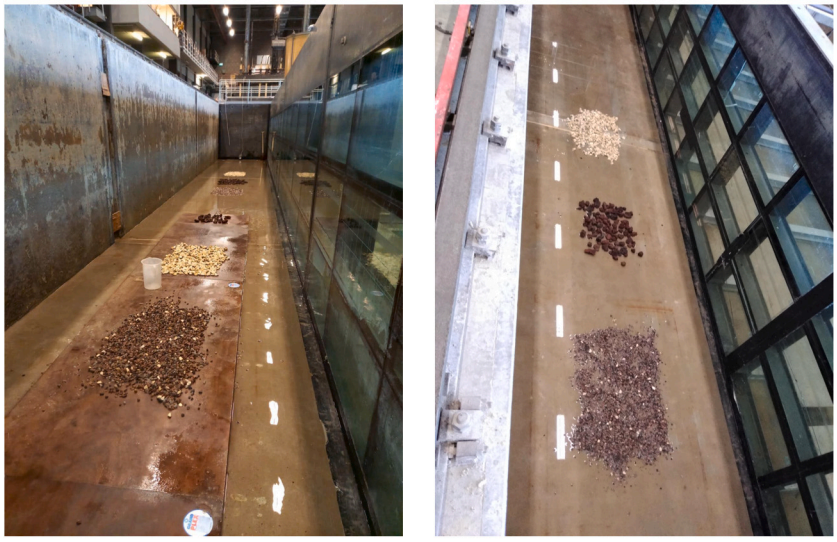

Fig. 16. First half (**left**) and second half of the collector path (**right**), in the case of a rigid bed.

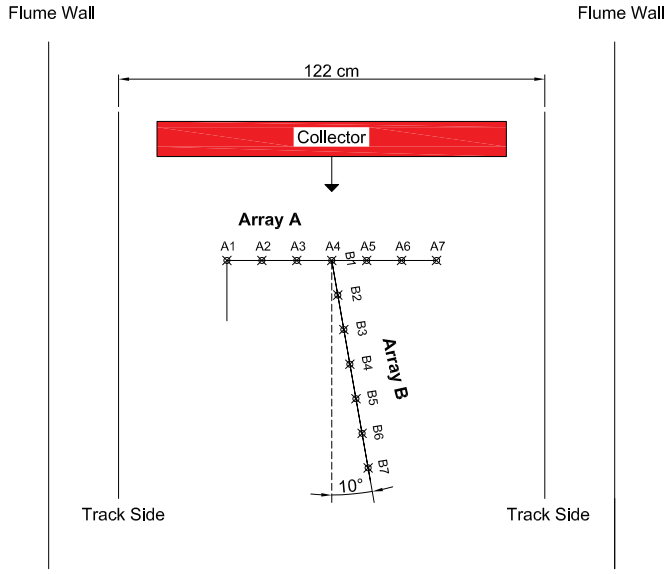

Fig. 17. Top view of the location of two arrays of pressure sensors placed at the flume bed; the markers refer to the position of sensors, which are spaced by a distance of 0.1 m; A4 = B1.

flowmeters of ±0.5% accuracy were used; one was placed at the pressure pipe to monitor the jet flow rate (or jet velocity), and the other was placed at the discharge pipe to monitor the flow rate of the discharged flow. Conductivity-type concentration meters (CCM) were calibrated and used to monitor the local sediment concentrations. CCM measures particle concentrations at a single point based on the conductivity change of a sediment-water mixture as a result of the change of the amount of suspended particles within the measuring volume [2].

As for the pressure, two arrays of pressure sensors (type: PDCR 810, measuring range: 1 bar, accuracy: ±0.1% BSL) were mounted at the flume bed to measure the pressure drop once the collector approaches or drives over the measuring points (see Fig. 17). Array A is parallel to the mouth of the jet. Array B is inclined by 10° to the perpendicular (the direction of flow), because the mouth of the collection duct is inclined by 10° to the mouth of the jet. This is simply due to the construction of the prototype that required the collection duct to be split into two to make room for the pump that would circulate the water. It is to be noted that it was not possible to have measurements along Array A and Array B simultaneously in the same experimental run due to the insufficient number of pressure sensors.

Besides the aforementioned sensors, two digital video cameras were employed to record the entire experimental run, in the case of using a sand bed. The first camera was positioned in front of the collector, while the second camera was fastened on one side of the collector. The view of both cameras was set on the sand bed to closely monitor the collection process of nodules. It was not possible to mount the cameras in the case of a rigid bed, since the collector was too close to the flume bed. The mobile carriage was equipped with a sensor to measure the forward velocity of the collector and a sensor to pinpoint the spatial start and end points of the measurement track.

4.4. Characterization of nodules and sand bed

Nodules

To study the influence of nodule size and geometry on the pick-up process, three types of nodules were used in the experiments (see Fig. 18). Here, the smallest, medium and largest nodules are referred to as red nodules, white nodules and lava nodules, respectively. Table 1 summarizes the characteristics of these nodules. It is worth noting that lava nodules have a wet density (2200 kg/m^3) comparable to the density of real polymetallic nodules (about 2000 kg/m^3). The settling velocity of single nodules was measured by allowing the nodules to fall freely in the flume and measuring the traveling distance and time.

Fig. 18. The three types of nodules used in the experiments; red nodules (**left**), white nodules (**middle**) and lava nodules (**right**).

Table 1
The characteristics of nodules used in the experiments. w_o, $\overline{w_0}$ and σ_{w_0} are the range, average and the standard deviation of the settling velocity of a single nodule, respectively.

Nodule	Size [mm]	Wet Density [kg/m^3]	w_0 [m/s]	$\overline{w_0}$ [m/s]	σ_{w_0} [m/s]
Red	8-16	2495	0.38-0.46	0.43	0.04
White	20-40	2567	0.33-0.81	0.54	0.16
Lava	40-80	2200	0.63-1.06	0.84	0.13

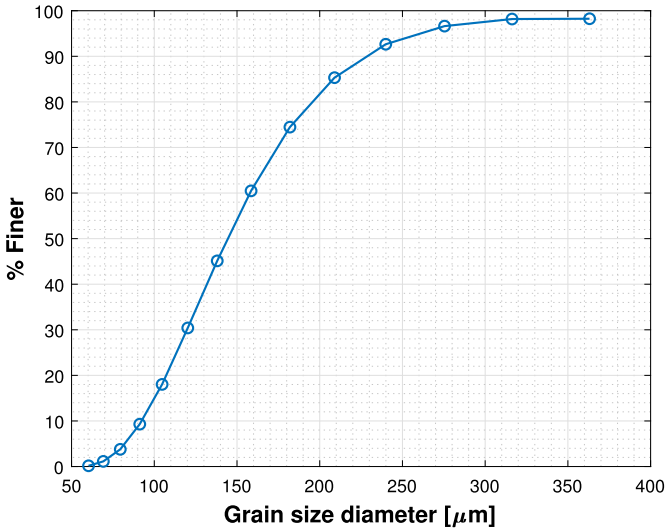

Fig. 19. Cumulative grain size distribution of the sand used in the experiments, as derived from the Laser Diffraction technique.

Table 2
The properties of the sand used in the experiments.

d_{10}	d_{30}	d_{50}	d_{60}
0.092 mm	0.120 mm	0.145 mm	0.158 mm

Sand bed

A fine sand (GEBA weiss) of d_{50} equal to 0.145 mm was used in the experiments. The cumulative grain size distribution of this sand was determined using the Laser Diffraction technique (see Fig. 19). The properties of the used sand are summarized in Table 2.

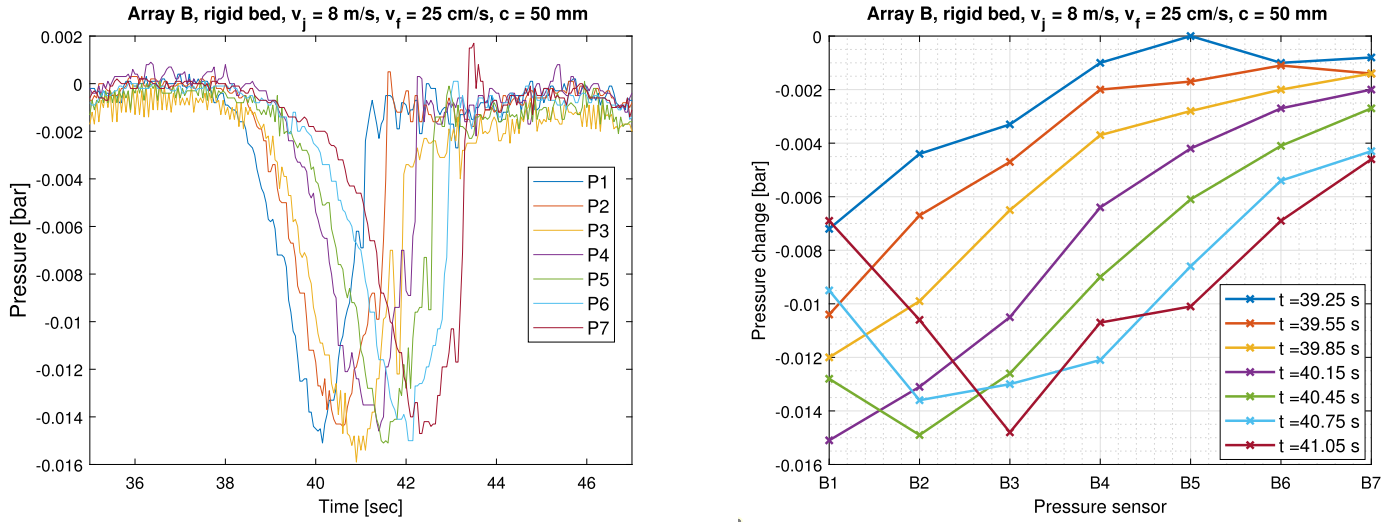

Fig. 20. Temporal evolution of pressure at the seven measuring points located along Array B (**left**). Spatial pressure distribution along Array B (**right**) (see Fig. 17).

4.5. Data processing

In this subsection, samples of the raw data are presented and data post-processing is described. The measurements were sampled with a frequency of 20 Hz. In the experimental work, we tested four different jet velocities: 6, 8, 10 and 12 m/s.

4.5.1. Pressure change under collector

To calculate the pressure change at the measuring points located along Array A and Array B, the pressure measurements taken before the movement of the collector were set to zero for all pressure sensors. The left panel of Fig. 20 demonstrates that there is a pressure drop of about 0.015 bar within a time span of 2 seconds (operational conditions of this experiment are reported on the same figure). The pressure distribution can be visualised by plotting multiple pressure profiles corresponding to different instances in time (Fig. 20 right).

4.5.2. Water entrainment

Following the continuity principle and assuming that the flow rate in the discharge pipes is similar, the flow rate of the net entrained water into the collection duct can be calculated Q_e as follows:

$$Q_e = Q_d - Q_j, \tag{1}$$

where Q_j is the volumetric flow rate through the jet and Q_d is the flow rate in the discharge pipes.

Fig. 21 depicts the temporal evolution of the flow rates Q_j, Q_d and Q_e in an experimental run when the collector drives forward with a velocity of 25 cm/s over the testing track. The time interval during which the collector was driving over a certain type of nodules was defined based on the video recordings and the measurements of the forward velocity of the collector. To study the effect of Q_e on the pick-up efficiency, the average value of Q_e was calculated for each type of nodules (see Section 4.6).

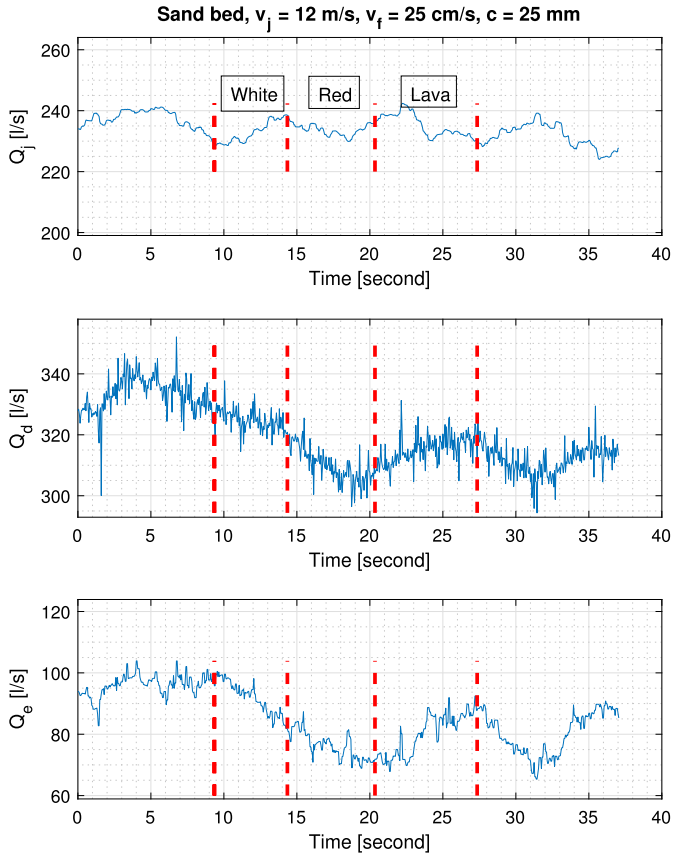

Fig. 21. Temporal change of Q_j, Q_d and Q_e during an experimental run. For comparison's sake, y-axis has the same length in the three sub-figures.

4.6. Experimental results

To investigate the effect of a certain parameter on the collection process, experimental runs were conducted in which the initial conditions were kept invariant while that parameter was varied. The primary parameters studied here are jet velocity, forward velocity, clearance and bed type. Here, the influence of these is first discussed based on the experimental results and followed by the presentation and discussion of the other experimental results.

4.6.1. Jet velocity

The pick-up efficiencies for each nodule type were calculated for experiments with different jet velocities (see Fig. 22). It can clearly be seen that higher jet velocities result in higher pick-up efficiencies (Fig. 22 left). This is because a higher jet velocity leads to a larger pressure gradient under the collector, thereby picking-up more nodules. To illustrate this, the maximum pressure drop under the collector at the measuring points along Array B for two runs of different jet velocities is plotted (see Fig. 23 left).

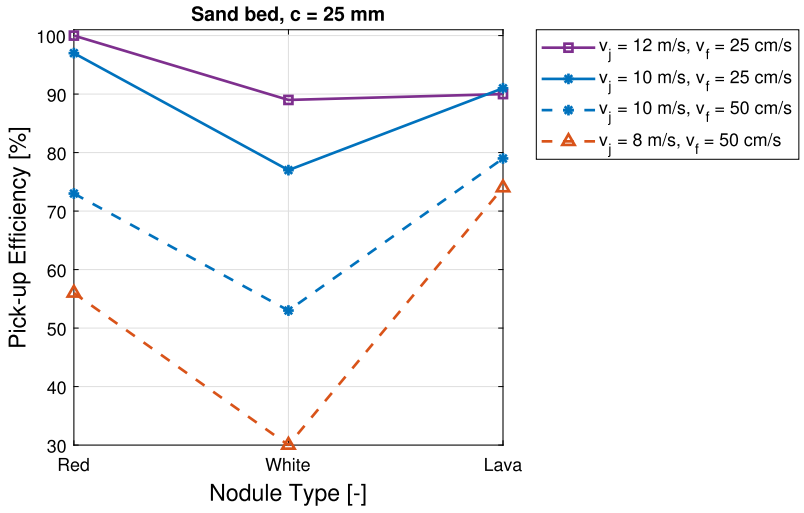

Fig. 22. Effect of jet velocity and forward velocity on the pick-up efficiency; v_j is jet velocity and v_f is the forward velocity of the collector.

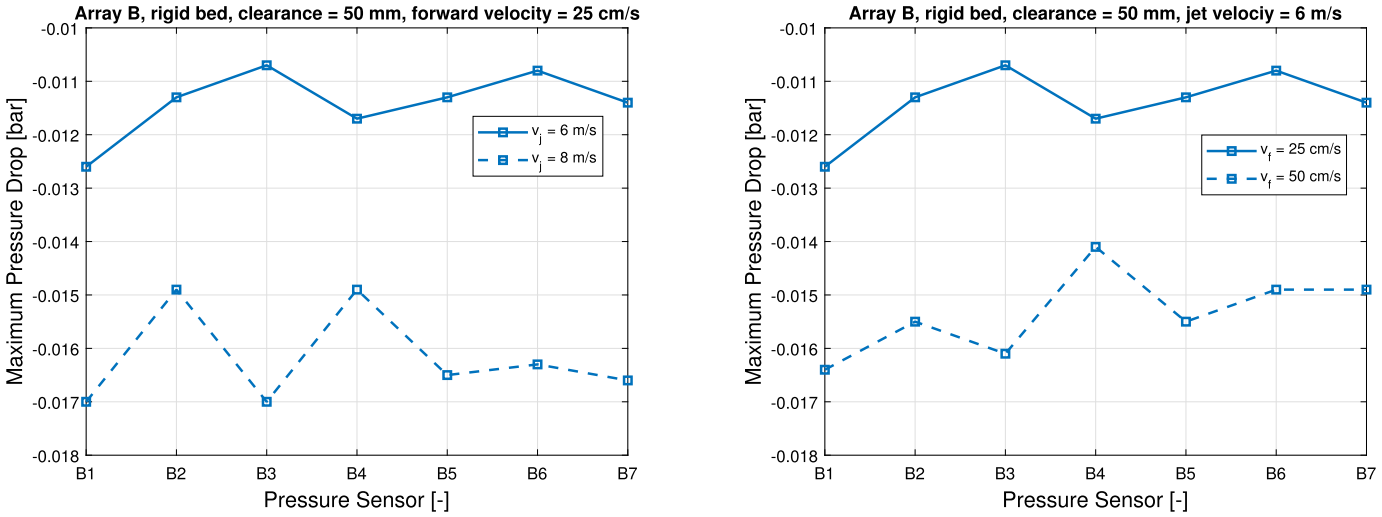

Fig. 23. Effect of jet velocity (**left**) and forward velocity (**right**) on the maximum pressure drop under the collector; v_j is jet velocity and v_f is the forward velocity of the collector.

Fig. 24 demonstrates that a higher jet velocity v_j results in a higher flow rate of the entrained water into the collection duct Q_e. It is to be noted that the entrained water promotes the pressure gradient under the collector, consequently improving the pick-up efficiency.

4.6.2. Forward velocity

In a similar manner to the analysis shown in the previous subsection, the effect of the forward velocity of the collector was explored. The experimental results show that a decreased forward velocity improves the pick-up efficiency (Fig. 22 left). This is attributed to the point that a lower forward velocity provides more time for the nodules to respond to the pressure gradient, and to be dislodged and subsequently collected.

The right panel of Fig. 23 depicts that a higher forward velocity results in a larger pressure gradient under the collector. This is because a higher forward velocity leads to a higher Q_e, as can be inferred from the results shown in Fig. 24. It can be concluded that a higher pressure gradient under the collector does not necessarily result in a higher pick-up efficiency. In other words, the available time for the nodules to respond to the pressure gradient is very crucial for the collection process; if the available time is insufficient, the nodules will not be picked-up even if the pressure gradient is adequate.

4.6.3. Clearance

The clearance under the rear cowl of the collection duct (hereinafter referred to as the "clearance") plays an influential role in the collection process. The experimental results show that a smaller clearance leads to a higher pick-up efficiency (see Fig. 25). This is because a smaller clearance generates a larger suction force as can be inferred from the pressure change illustrated in Fig. 26 left. On top of that, a smaller clearance means the center of gravity of these nodules is closer to the underside of the collector, resulting in a higher pick-up efficiency.

The right panel of Fig. 26 shows that the smaller the clearance the lower the flow rate of the entrained water. This makes sense as a large clearance means a larger space for water entrainment. We did not test negative clearances, because we wanted to collect the nodules hydraulically without digging into the bed.

4.6.4. Bed type

Two bed types were used in the experimental work: rigid bed (concrete or wood) and a sand bed. Although the center of gravity of nodules, in the case of a sand bed, is closer to the collector's underside, it is found that a sand bed results in a lower pick-up efficiency than a rigid bed (see Fig. 27). In the case of a rigid bed, the nodules were placed directly on the bed, while they were half buried into the sand bed, cre-

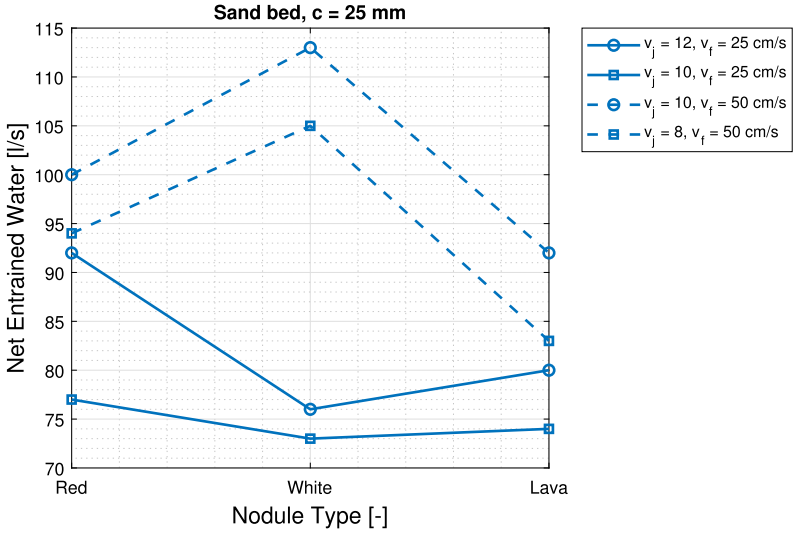

Fig. 24. Effect of jet velocity v_j and forward velocity v_f on the volumetric flow rate of the net entrained water into the collection duct Q_e.

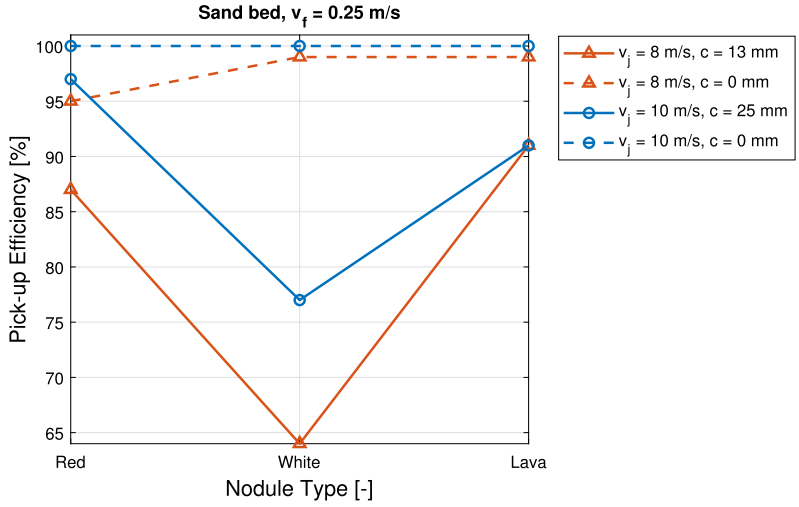

Fig. 25. Effect of clearance on the pick-up efficiency; v_j is jet velocity and c is the clearance under the rear cowl of the collection duct.

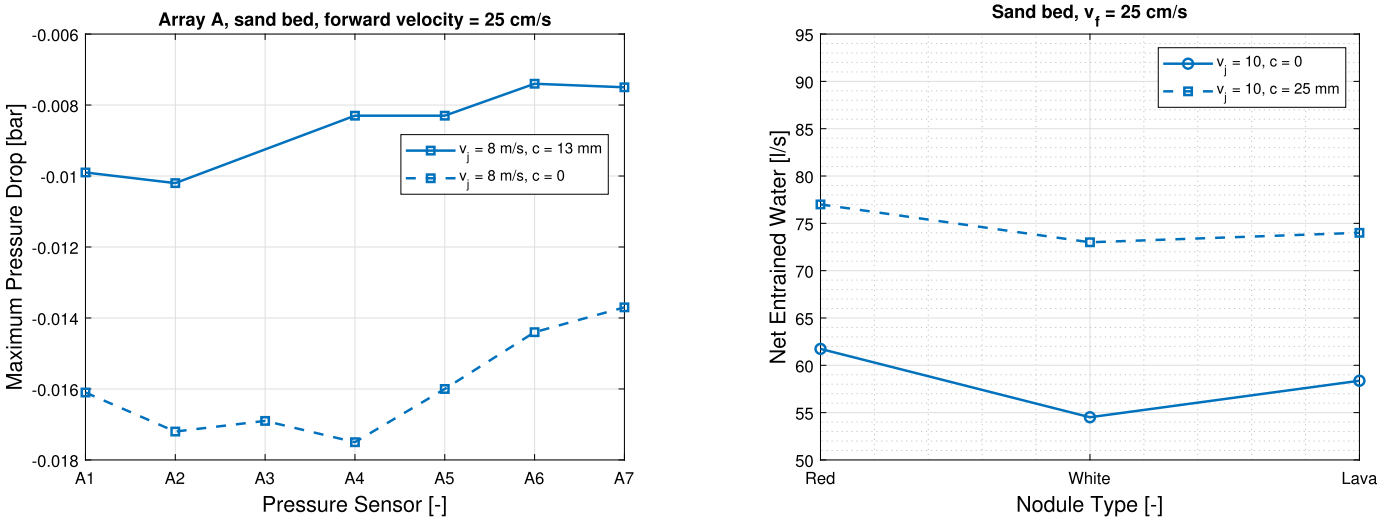

Fig. 26. Effect of clearance under the rear cowl of the collection duct c on the pressure gradient under the collector (**left**) and on the volumetric flow rate of the net entrained water into the collection duct Q_e (**right**); v_j is jet velocity and v_f is the forward velocity.

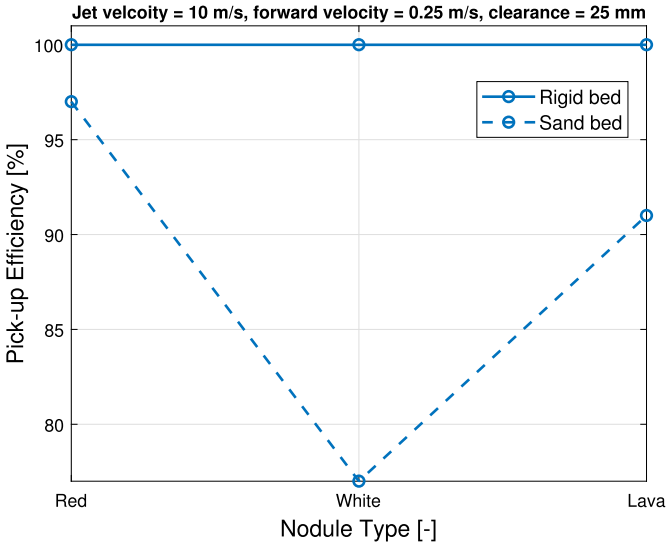

Fig. 27. Effect of bed type on the pick-up efficiency.

ating friction between them and sand, which acts as a stabilizing force. Besides, the nodules are fully exposed to the flow under the collector in the case of a rigid bed, resulting in a higher lift force applied on the nodules, in contrast to the case of a sand bed. In addition, and most importantly, the collector quickly pulls out the nodules from the sand bed, potentially leading to the build-up of a negative pressure, which also acts as a stabilizing force. Whether a clay bed leads to a better pick-up efficiency than a sand bed or not remains an open question. Nevertheless, we expect that the deep seabed would result in a better pick-up efficiency, as the top layer of sediment is semi-liquid [9,10].

4.6.5. Pick-up efficiency

To select the optimal operational conditions of the collector, the pick-up efficiency of the tested operational conditions in the case of a sand bed is shown in Fig. 28 for each type of nodules. This figure includes valuable data that can be used to define directions for collector optimization. The results distinctly demonstrate that the operational conditions involving a zero clearance lead to the best pick-up efficiencies. In descending order, the overall pick-up efficiency of these best cases are 100%, 100% and 98%. The lowest overall pick-up efficiency between all tested cases is 53%. The results also show that lava nodules, in almost all tested operational conditions, have the highest pick-up efficiency among the tested nodules. This could be attributed to the fact that lava nodules have the largest grain size, meaning that the center of gravity of these nodules is closer to the underside of the collector, resulting in a higher pick-up efficiency. It is found that the pick-up efficiency of the white nodules is the lowest in the vast majority of the tested operational conditions. In this respect, it is worth mentioning that the white nodules were angular and flat, in contrast to the other tested nodules, resulting in a poorer variation in pressure under the collector and subsequently a lower pick-up efficiency. It remains to select the optimal operational conditions based on their productivity and feasibility in practice. Concerning the latter, the main issue would be how good the position of the collector can be controlled to maintain a zero clearance.

4.6.6. Sediment concentration

To measure the sediment concentration of the sediment-water mixture, multiple CCMs were mounted inside the collector. The raw measurements of all CCMs were outside the range of the raw data obtained throughout the calibration process, indicating that the sediment concentration is lower than the range within which the CCM is reliable. To double check, a siphon tube, together with a small suction pump, was used to obtain suspended sediment samples from two different locations, namely the exit of the discharge pipe and the collection duct. Following that, these samples were weighed and dried to calculate the sediment concentration. In agreement with the indication of the CCMs measurements, the sediment concentration of the siphon samples ranged between 0.1% and 0.7%. This low concentration implies that the erosion rate of the sand bed was also low, which is in line with the visual observations.

4.6.7. Pressure under the collector

The measurements of the pressure sensors along Array A and Array B demonstrate the pressure distribution at the bed when the collector is nearby or drives over the measuring points.

Array A

The pressure distribution seems to be symmetric around the pressure sensor A4 (Fig. 29 right), which was mounted in the middle of the

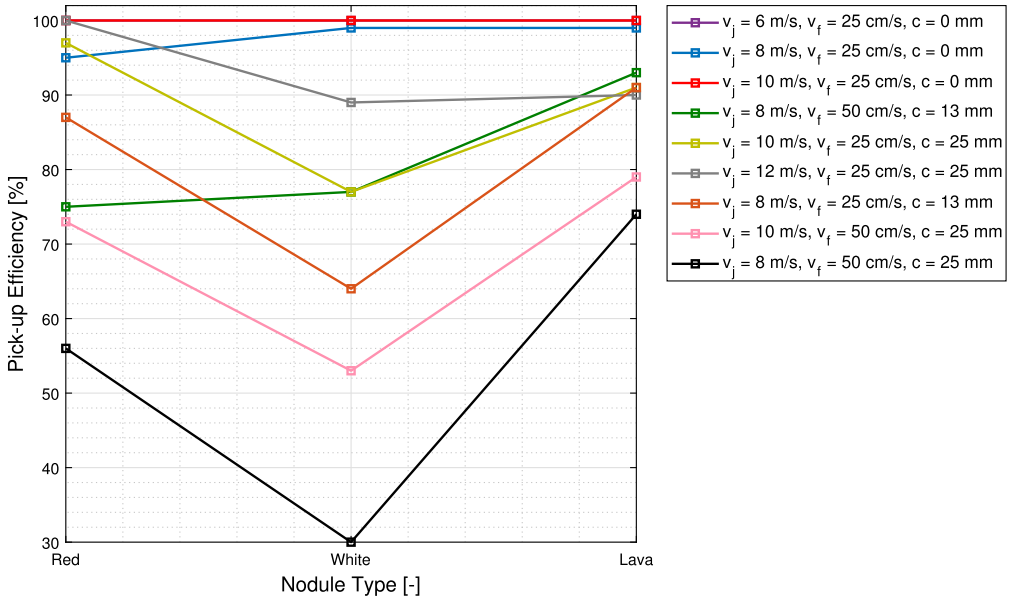

Fig. 28. Pick-up efficiency of the tested operational conditions in the case of a sand bed.

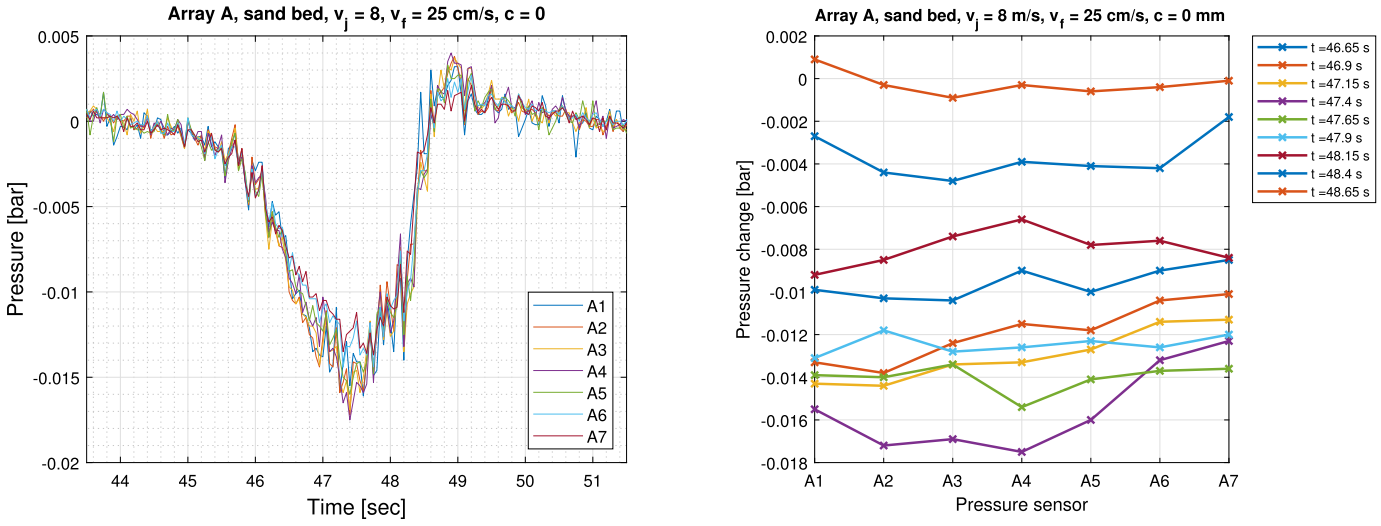

Fig. 29. Temporal pressure distribution along Array A at the bed.

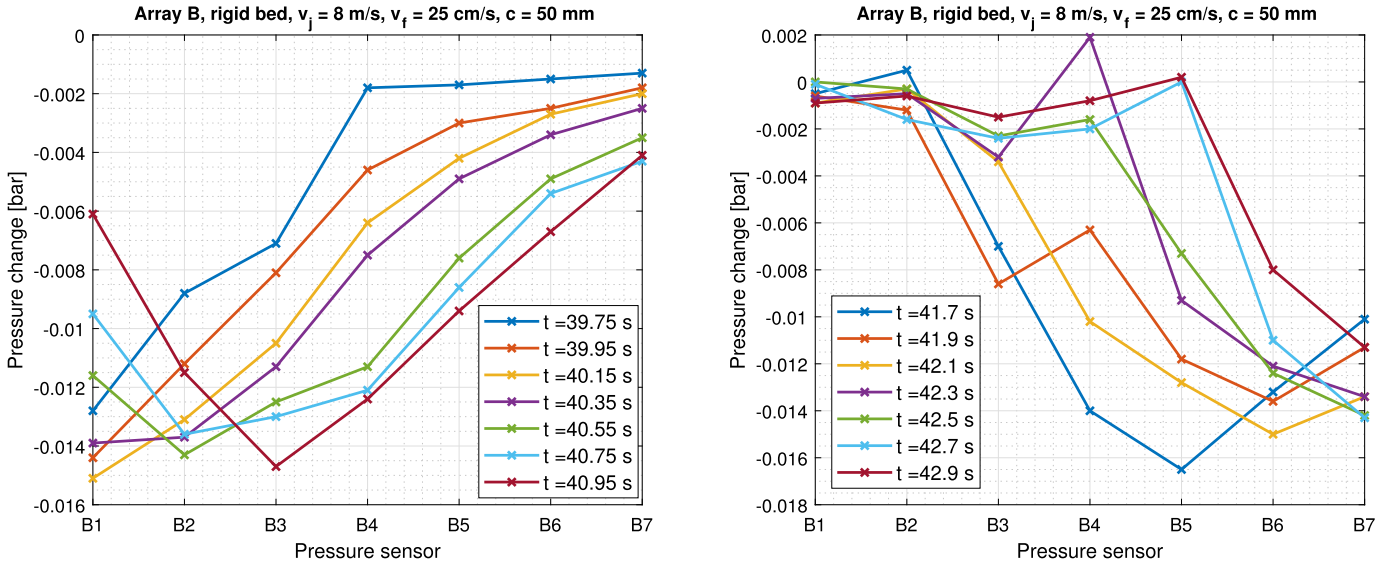

Fig. 30. Temporal pressure distribution along Array B at the bed.

testing track. It is to be noted that not all pressure profiles show symmetry, which can be attributed to the sensitivity of the sensors. In terms of the pick-up process, no observations conflicting with the pressure symmetry were made during the experiments.

Array B

When the collector approaches the sensors, the suction is the highest at sensor B1 and reduces towards sensor B7 (Fig. 30 left). Shortly after that, when the collector drives forward, the pressure distribution flips along Array B, so the suction becomes the highest at B7 and the lowest at B1 (Fig. 30 right). It is also observed that the pressure changes gradually when the collector approaches the measuring points, whereas the pressure changes abruptly returning to the reference value, when the collector drives away from the pressure sensors (see Fig. 20 right).

5. Conclusion

A Coandă-effect-based design of a polymetallic nodule collector was presented and tested through numerical simulations and a series of full-scale experiments. In the latter, several different operational conditions were tested, evidencing the functionality of the collector and providing important quantitative data for selecting the optimal operational conditions. The experimental results show the effectivity of our design, since high pick-up efficiency and low disturbance of the bed were achieved. It is revealed that a higher jet velocity results in a higher pick-up efficiency. We have tested two forward velocities and the higher one resulted in a lower pick-up efficiency. The exposure time of the applied force to pick up nodules is found to be crucial; if the exposure time is inadequate, the nodules will not be picked-up even if the applied force is adequate. The experimental results highlight the vital role of the clearance under the rear cowl of the collection duct; a smaller clearance results in a higher pick-up efficiency reaching 100%.

CRediT authorship contribution statement

Conceptualization and Methodology: All authors; Writing of Section 3: Dhruv Mehta; Writing of the other sections: Said Alhaddad; Execution of experiments: Said Alhaddad and Rudy Helmons; Analysis of experimental results: Said Alhaddad; Analysis of numerical results:

Dhruv Mehta; Funding acquisition, Reviewing and Editing: Rudy Helmons.

Declaration of competing interest

The authors declare that they have no known competing financial interests or personal relationships that could have appeared to influence the work reported in this paper.

Data availability

Data will be made available on request.

Acknowledgement

This study was conducted as a part of the Blue Harvesting project, which is funded by the European Institute of Innovation and Technology, EIT Raw Materials under Project Agreement 18138, Specific Grant Agreement No. [EIT/RAW MATERIALS/SGA2019/1].

References

[1] B. Agarwal, P. Hu, M. Placidi, H. Santo, J.J. Zhou, Feasibility Study on Manganese Nodules Recovery in the Clarion-Clipperton Zone, vol. 2, University of Southampton, 2012.
[2] S. Alhaddad, R.J. Labeur, W. Uijttewaal, Large-scale experiments on breaching flow slides and the associated turbidity current, J. Geophys. Res., Earth Surf. 125 (2020) e2020JF005582.
[3] A. Boetius, M. Haeckel, Mind the seafloor, Science 359 (2018) 34–36.
[4] T. Brockett, Nodule collector subsystem', in: Workshop on Proposed Technologies for Deep Seabed Mining of Polymetallic Nodules: International Seabed Authority Meeting, 1999, pp. 67–93.
[5] S. Cho, S. Park, J. Oh, C. Min, H. Kim, S. Hong, J. Jang, T.H. Lee, Design optimization of deep-seabed pilot miner system with coupled relations between constraints, J. Terramech. 83 (2019) 25–34, https://doi.org/10.1016/j.jterra.2019.01.003.
[6] K. De Bruyne, H. Stoffers, S. Flamen, H. De Beuf, C. Taymans, S. Smith, K. Van Nijen, A Precautionary Approach to Developing Nodule Collector Technology, Springer International Publishing, Cham, 2022, pp. 137–165.
[7] E. van Doorn, J. Laugesen, M. Haeckel, N. Mestre, F. Skjeret, A. Vink, Risk Assessment for Deep-Seabed Mining, Springer International Publishing, Cham, 2022, pp. 497–526.
[8] M. Elerian, S. Alhaddad, R. Helmons, C. van Rhee, Near-field analysis of turbidity flows generated by polymetallic nodule mining tools, Mining 1 (2021) 251–278.
[9] B. Grupe, H.J. Becker, H.U. Oebius, Geotechnical and sedimentological investigations of deep-sea sediments from a manganese nodule field of the Peru basin, Deep-Sea Res., Part 2, Top. Stud. Oceanogr. 48 (2001) 3593–3608.
[10] GSR, Environmental Impact Statement: Small-scale testing of nodule collector components on the seafloor of the Clarion-Clipperton Fracture Zone and its environmental impact, Technical Report, 2018.
[11] S. Haalboom, T. Schoening, P. Urban, I.Z. Gazis, H. de Stigter, B. Gillard, M. Baeye, M. Hollstein, K. Purkiani, G.J. Reichart, L. Thomsen, M. Haeckel, A. Vink, J. Greinert, Monitoring of anthropogenic sediment plumes in the Clarion-Clipperton Zone, NE equatorial Pacific Ocean, Front. Mar. Sci. 9 (2022) 882155, https://doi.org/10.3389/fmars.2022.882155.
[12] J.R. Hein, A. Koschinsky, T. Kuhn, Deep-ocean polymetallic nodules as a resource for critical materials, Nat. Rev. Earth Environ. 1 (2020) 158–169.
[13] S. Hong, J.S. Choi, J.H. Kim, C.K. Yang, et al., Experimental study on hydraulic performance of hybrid pick-up device of manganese nodule collector, in: Third ISOPE Ocean Mining Symposium, International Society of Offshore and Polar Engineers, 1999.
[14] S. Hong, J.S. Choi, J.Y. Shim, et al., A kinematic and sensitivity analysis of pick-up device of deep-sea manganese nodule collector, in: Second ISOPE Ocean Mining Symposium, International Society of Offshore and Polar Engineers, 1997.
[15] IEA, Total mineral demand for clean energy technologies by scenario, 2020 compared to 2040, Technical Report, 2022.
[16] H. Jia, J. Yang, X. Su, Q. Xia, K. Wu, Theoretical prediction on hydraulic lift of a Coandă effect-based mining collector for manganese nodule, Energies 15 (2022), https://doi.org/10.3390/en15176345.
[17] J. McFarlane, T. Brockett, J. Huizingh, Analysis of Mining Technologies Developed in the 1970s and 1980s, International Seabed Authority, Kingston, 2008.
[18] NORI, Collector Test Study, Environmental Impact Statement, Testing of polymetallic nodule collector system components in the NORI-D contract area, Clarion-Clipperton Zone, Pacific Ocean, Technical Report, 2021.
[19] J. Parianos, I. Lipton, M. Nimmo, Aspects of estimation and reporting of mineral resources of seabed polymetallic nodules: a contemporaneous case study, Minerals 11 (2021) 200.
[20] T. Radziejewska, K. Mianowicz, T. Abramowski, Natural Variability Versus Anthropogenic Impacts on Deep-Sea Ecosystems of Importance for Deep-Sea Mining, Springer International Publishing, Cham, 2022, pp. 281–311.
[21] K.J. Schulz, J.H. DeYoung, R.R. Seal, D.C. Bradley, Critical mineral resources of the United States: economic and environmental geology and prospects for future supply, Geol. Surv. (2018).
[22] P. Weaver, J. Aguzzi, R. Boschen-Rose, A. Colaço, H. de Stigter, S. Gollner, M. Haeckel, C. Hauton, R. Helmons, D. Jones, H. Lily, N. Mestre, C. Mohn, L. Thomsen, Assessing plume impacts caused by polymetallic nodule mining vehicles, Mar. Policy 139 (2022) 105011, https://doi.org/10.1016/j.marpol.2022.105011.
[23] N. Yang, H. Tang, Several considerations of the design of the hydraulic pick-up device, in: Fifth ISOPE Ocean Mining Symposium, International Society of Offshore and Polar Engineers, 2003.
[24] Z. Yue, G. Zhao, L. Xiao, M. Liu, Comparative study on collection performance of three nodule collection methods in seawater and sediment-seawater mixture, Appl. Ocean Res. 110 (2021) 102606.
[25] G. Zhao, L. Xiao, Z. Yue, M. Liu, T. Peng, W. Zhao, Performance characteristics of nodule pick-up device based on spiral flow principle for deep-sea hydraulic collection, Ocean Eng. 226 (2021) 108818, https://doi.org/10.1016/j.oceaneng.2021.108818.
[26] S. Zhao, F. Liu, Study of deep-sea mining technique in Germany, Metal Mine (1995) 14–17.